Modeling of the effect of intentionally introduced traps on hole transport in single-crystal rubrene

Javier Dacuña,[1] Amit Desai,[2] Wei Xie,[3] and Alberto Salleo[2,*]

[1]*Department of Electrical Engineering, Stanford University, Stanford, California 94305, USA*

[2]*Department of Materials Science and Engineering, Stanford University, Stanford, California 94305, USA*

[3]*Department of Chemical Engineering and Materials Science, University of Minnesota, Minneapolis, Minnesota 55455, USA*

(Received 24 February 2014; revised manuscript received 4 May 2014; published 5 June 2014)

Defects have been intentionally introduced in a rubrene single crystal by means of two different mechanisms: ultraviolet ozone (UVO) exposure and x-ray irradiation. A complete drift-diffusion model based on the mobility edge (ME) concept, which takes into account asymmetries and nonuniformities in the semiconductor, is used to estimate the energetic and spatial distribution of trap states. The trap distribution for pristine devices can be decomposed into two well defined regions: a shallow region ascribed to structural disorder and a deeper region ascribed to defects. UVO and x ray increase the hole trap concentration in the semiconductor with different energetic and spatial signatures. The former creates traps near the top surface in the 0.3–0.4 eV region, while the latter induces a wider distribution of traps extending from the band edge with a spatial distribution that peaks near the top and bottom interfaces. In addition to inducing hole trap states in the transport gap, both processes are shown to reduce the mobility with respect to a pristine crystal.

DOI: 10.1103/PhysRevB.89.245302 PACS number(s): 72.80.Le, 71.20.Rv

I. INTRODUCTION

Organic semiconductors have attracted significant interest in recent years for applications in low-cost and large area electronics [1–5]. Their unique properties make them compatible with high throughput roll-to-roll printing and low temperature deposition, thus allowing the utilization of inexpensive and flexible substrates.

Although some commercial applications using organic semiconductors, such as OLED displays, are already available; the utilization of organic materials in many other commercial devices is still a challenge due to the limitations and degradation of their electronic properties. The importance of obtaining a deeper understanding of the factors limiting or degrading the performance of organic semiconductors cannot be overemphasized. One way to further investigate the effect that different types of defects have on the electrical properties of organic materials is by deliberately introducing defects and analyze how the electrical characteristics change. Inducing defects in a controlled manner, and the ability to correlate them to the effect on the transport properties, will be instrumental in the understanding of how environmental factors or processing conditions may affect the performance of organic semiconductor devices. The utilization of organic single crystals for this purpose is convenient, since their low intrinsic defect density makes it much simpler to compare their properties before and after any damage.

This work presents a comparison of the effect of two different model defects on rubrene single crystals: those induced by UVO (ultraviolet ozone) exposure, and those induced by x-ray irradiation. These two processes are performed to intentionally introduce defects with different spatial distributions—i.e., surface versus bulk—thus affecting the semiconductor electrical properties in different ways. A numerical model is used to analyze the current-voltage characteristics in hole-only diodes before and after introducing defects, leading to different spatial and energetic signatures, which suggests fundamentally different origin for the induced trap states.

II. MATERIALS AND METHODS

Rubrene single platelike crystals, with thickness ranging from 0.8 to 1 μm, were grown by horizontal physical vapor transport [6]. Ultrapure argon was used as the carrier gas. Typical growth temperature was 300 °C. Platelike crystals a few millimeters wide and long were collected after a 30 min growth and were immediately laminated on a clean Si wafer with prefabricated Cr (3 nm)/Au (30 nm) electrodes. A bottom contact was formed by spontaneous adhesion of the crystal onto a gold coated substrate. The top contact, in contrast, was prepared by carefully depositing a drop of water-based graphite on top of the rubrene crystal with a 25 μm gold wire attached to provide an electrical contact without stressing the delicate crystal surface. Before performing any measurement, the top contacts were allowed to dry for ∼30 min. Water-based graphite was selected as the top electrode material due to the high quality of the contact—in terms of low local trap concentration estimated through the proposed model—compared to silver ink (Ted Pella Leitsilber 200) and isopropanol-based graphite. Repeated measurements of the same device show that multiple temperature cycles do not affect transport in the out-of-plane direction. With the help of a profilometer, thickness was estimated by averaging measurements at different points around the edges. Measured thickness are in the range from 0.8 to 1 μm, with an estimated error of less than 10%. The contact area, on the other hand, was measured graphically from an optical micrograph.

Defects in the crystals were introduced by means of two different mechanism: UVO exposure and x-ray irradiation. UVO exposure was performed by exposing the top surface of the rubrene crystal to UVO for 30 s, enough time to create a measurable change in the IV characteristics. The crystal was exposed to UVO before depositing the top contact but after lamination onto the gold-coated substrate, so UVO exposure is limited to the top surface of the crystal. X-ray-induced defects

*asalleo@stanford.edu

were created by exposing the crystal to the x-ray beam of a diffractometer (Cu-$K\alpha$, 45 kV, 40 mA) for periods of 5000 s. Irradiation was performed either before or after top contact deposition. Specific details are reported where relevant.

III. UVO-INDUCED DEFECTS

Rubrene is one of the best organic semiconductors to date, with reported mobilities as high as 20–40 cm^2/V s [7]. Naturally oxidized rubrene has been shown to contain as much as 1% rubrene endoperoxide ($RubO_2$) near the surface [8]. Such a high concentration may affect the electrical properties of rubrene devices, specially in geometries where transport is particularly sensitive to the surface. However, despite multiple studies trying to understand the effect of oxygen in rubrene, the role of oxidation is still unclear.

Mitrofanov *et al.* reported that oxidation of rubrene creates a well defined photoluminescence (PL) peak located 250 meV above the valence band (VB) [8]. The appearance of the PL peak is correlated with an increase in the dark and photocurrent (PC) of rubrene crystals, leading to the conclusion that oxidation of rubrene creates acceptor states in the gap. In the same work, several possible mechanisms for the creation of the oxygen-related states are hypothesized: perturbation of a rubrene molecule by the presence of a neighboring oxygen molecule; formation of a rubrene peroxide molecule; or a rubrene molecule perturbed by the presence of a neighboring rubrene peroxide molecule.

In contrast, temperature dependent SCLC spectroscopy (TD-SCLC) was used by Krellner *et al.* to analyze the effect of oxygen in rubrene [9]. The authors showed that the formation of $RubO_2$ (either by illuminating the rubrene crystal with visible light under oxygen atmosphere, or by exposing the crystal in the dark to molecular oxygen excited with UV light) creates states at 0.27 eV above the VB. Although the obtained characteristic energy is close to 250 meV, we note that the states were reported to be donorlike—i.e., hole traps—instead of acceptors, thus hindering hole transport instead of increasing dark and PC due to a doping effect. These results are consistent with the decrease in PC reported by Najafov *et al.* after illuminating a rubrene crystal in an oxygen atmosphere [10].

Other groups, instead, have reported that oxidation of rubrene does not create any in-gap state—neither donor nor acceptor—since the incorporation of oxygen causes the HOMO of rubrene to shift down in energy by ∼1 eV [11]. The creation of in-gap states, in this case, has been hypothesized to be caused by the disruption of the long-range periodicity due to the creation of point defects by the oxidized molecules. In a different work, it has been stated that the formation of $RubO_2$ itself does not create in-gap states due to the deeper HOMO and wider band gap of oxidized molecules; however, the polar character of $RubO_2$ may lift the HOMO level of neighboring rubrene molecules forming states in the gap [12].

Note, however, that many of these works use different measurement techniques and device configurations in which charge transport may occur along different crystal orientations or may be sensitive to different regions of the crystal (bulk versus surface). Hence direct comparison of the results is often difficult.

A. Electrical characterization

The IV characteristics were measured in vacuum and in the dark at different temperatures. The minimum temperature in the data set is directly related to the resolution that can be achieved in the estimation of the energetic distribution of traps. Simply, the ability to estimate the energetic trap distribution is based on how trap states at different energies are progressively filled or emptied as the Fermi level moves through the DOS by sweeping the applied voltage. According to the Fermi distribution, the lower the temperature, the sharper the transition between empty and occupied states, and hence the better the resolution. Unfortunately, graphite contacts tend to detach from the rubrene crystal after a few temperature cycles if they are cooled to very low temperatures. For this reason, the temperature range was limited to 240–320 K.

A contact (C1) was deposited on top of a pristine rubrene crystal (crystal #5), forming the first device. Figure 1 presents the results of a set of temperature dependent measurements for device #5 C1. The IV curves at different temperatures are clearly asymmetric, i.e., the magnitude of the current for forward (injecting holes from the top contact) and reverse (injecting holes from the bottom contact) applied voltage is different. In particular, injection from the top contact shows an almost temperature independent current for voltages above 2–3 V, suggesting that most of the traps are filled and the Fermi level is close to the ME. This behavior confirms the high quality—in terms of trap concentration—of the water-based graphite contact.

The crystal was then exposed to UVO for 30 s and a new contact C2 was deposited afterwards. Then, both devices (C1 and C2) were measured every 48 h for a total of 4 days. The devices were stored in a nitrogen atmosphere and in the dark, between each measurement.

No significant change was observed on the IV measurements of device C1 before and after UVO. Since C1 was deposited before UVO exposure, the graphite layer on top of the rubrene crystal protected the semiconductor, thus the effect on the IV characteristics is negligible.

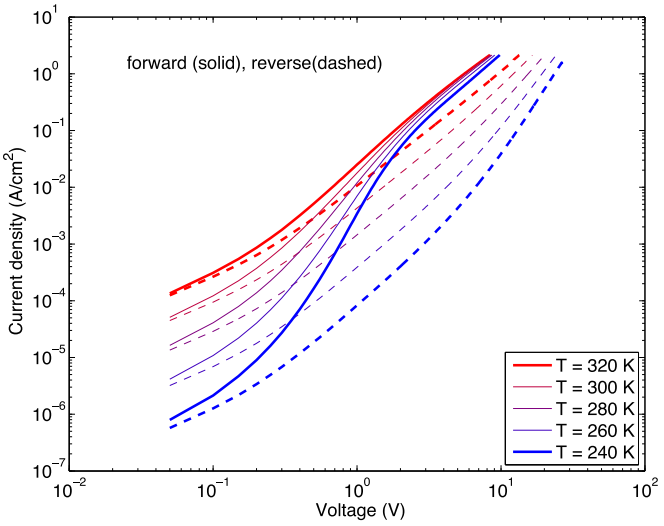

FIG. 1. (Color online) Temperature dependent IV characteristics for pristine device #5 C1.

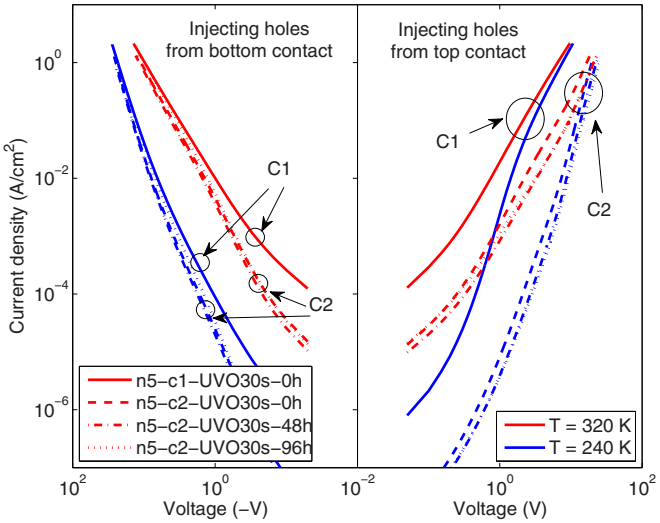

FIG. 2. (Color online) Temperature dependent IV characteristics for crystal #5 device C1 before UVO and C2 after UVO.

In contrast, the degradation on the current for C2 is clear when compared to C1 in Fig. 2. In particular for positive voltages, when holes are injected from the top contact, the current decreases by more than one order of magnitude and the trap-filled regime is not reached until biases larger than ∼10 V. Depositing several contacts on the same crystal after several days without further exposure to UVO did not show any significant degradation, thus confirming that the decrease in current seen in Fig. 2 is indeed caused directly by UVO. In contrast, changes in the negative bias region are minimal and are a consequence of the linearity of the device at $V \to 0$.

B. Data analysis

A numerical drift-diffusion model was used to analyze the effect of UVO on the electronic properties of the material. This model has been previously validated by estimating the energetic and spatial distribution of traps in organic materials from temperature dependent SCLC data [13,14]. In addition, confidence intervals were obtained for all relevant parameters to assess the accuracy of the estimated values. Although a detailed description of the model and calculation of the confidence intervals is given elsewhere [13,14], a summary of the main concepts and relevant parameters is given below for completeness.

Charge transport is modeled using the mobility edge (ME) model; which assumes that holes occupying states below the ME drift under the influence of an electric field with a constant mobility μ_0, while holes occupying states above ME are effectively trapped. The density of states is defined as the product $f(E)g(x)$, where $f(E)$ and $g(x)$ characterize the energetic and spatial dependence of the trap distribution, respectively. $f(E)$ can be either a Gaussian or a piecewise exponential function (PWE), i.e., the DOS is discretized and varies exponentially in between every two neighboring energy points, as shown in Fig. 3(a).

The spatial distribution can be uniform through the device or can decay exponentially from either (or both) contacts towards the bulk of the semiconductor as depicted in Fig. 3(b).

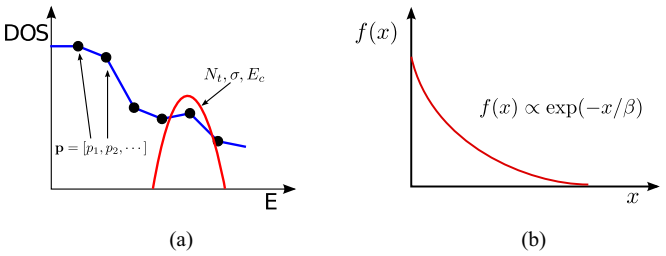

FIG. 3. (Color online) Model parameters: (a) Energy dependence of the density of trap states, arbitrary or Gaussian shape; and (b) spatial dependence of the density of trap states, decaying exponentially from the contact(s) to the bulk.

Due to the nature of the experiment, not all the parameters are expected to change after UVO exposure, hence only a subset of the parameters are optimized for each case.

In particular, fitting the IV characteristics for #5 C1 (pristine) required us to account for the free carrier mobility μ_0, a bulk (uniform in space) piecewise exponential DOS, and a local Gaussian DOS near the bottom contact (exponentially decaying from the bottom contact to the center of the semiconductor) [13,14]. The DOS at the band edge of the rubrene crystal has been calculated in the literature [15] as 10^{21} cm^{-3} eV^{-1}. This value, which corresponds to the value of the arbitrary PWE DOS at $E = 0$ eV, is fixed in the model.

The energetic barriers at each contact—given by the different workfunction of the material—were originally included as optimization parameters, but results were not sensitive to their specific value as long as they do not limit current injection (i.e., as long as the current is limited by the intrinsic or induced trap concentration and not by injection from the contact to the semiconductor). Since injection limited current was not observed for any of the devices, we fixed both energy barriers such that they do not limit the current at any temperature for any of the devices. By using the same value in all the simulations, pristine and UVO exposed, we assume that any difference in the IV characteristics induced by UVO is due to changes in mobility and trap concentration rather than on the band alignment at the contacts.

The asymmetry seen in Fig. 1 between forward and reverse bias is accounted for by a local Gaussian concentration of traps, leading to a slightly higher trap concentration near the bottom interface. Although we cannot rule out the possibility of a higher trap density near the top interface, including an extra concentration of traps near the top contact in the model converged to a very small amount, thus it was not considered in the final fit. After optimizing all the parameters, profile likelihood confidence intervals are calculated [13,16,17]. The confidence intervals are a graphical representation of the uncertainty inherent to each parameter. They depend on the measurement noise and on the correlations between the parameters—i.e., how the variation in one parameter can be compensated by changes in the remaining parameters, leading to very little change in the IV characteristics.

The model is able to reproduce the whole set of temperature dependent IV measurements as shown in Fig. 4.

Device C2, being on the same crystal #5, is expected to have the same intrinsic properties of the material as measured under

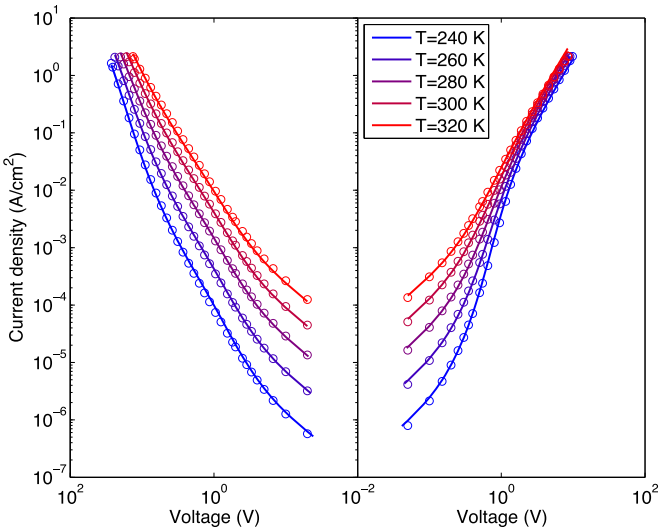

FIG. 4. (Color online) Comparison of measurements (circles) and model fit (solid lines) for crystal #5 C1 at different temperatures and bias conditions.

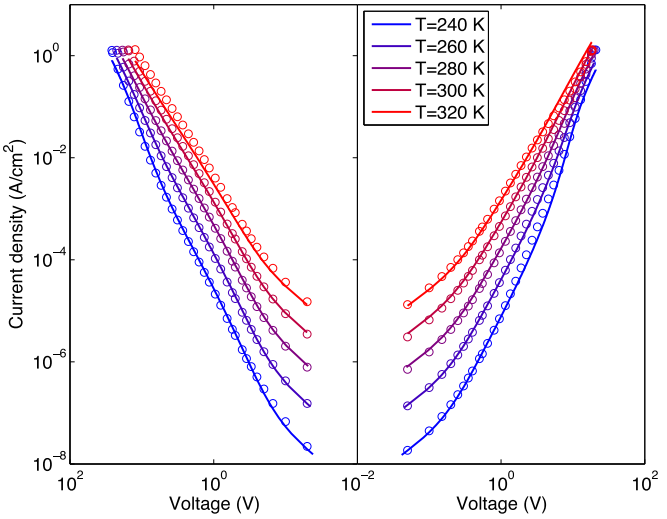

FIG. 5. (Color online) Comparison of measurements (circles) and model fit (solid lines) for crystal #5 C2 at different temperatures and bias conditions after exposure of the rubrene crystal to UVO.

C1, aside from changes induced by having exposed the top surface to UVO. For this reason, all the parameters estimated for #5 C1—mobility and DOS—were fixed. In addition to the fixed parameters, an extra arbitrary DOS was defined to account for the states that might have been created by UVO.

In this case, the extra DOS is not uniform in space but has a spatial dependence given by

$$g(x) = \frac{\gamma_b}{\beta_b}\exp(-x/\beta_b) + \frac{\gamma_t}{\beta_t}\exp[-(L-x)/\beta_t], \quad (1)$$

where γ_b (γ_t) and β_b (β_t) define the amplitude and exponential decay of the bottom (top) contact trap distribution. Note that $\beta \gg L$ leads to a nearly uniform distribution in the range 0–L, thus the spatial dependence of the trap distribution, as defined in (1), can account for all spatial distributions from completely uniform in space, to very localized near the contacts. The energetic distribution of the UVO-induced traps is assumed to be the same for all x. After optimizing the extra DOS, the model also reproduces the whole temperature dependent IV measurements for the UVO exposed device (Fig. 5).

The estimated μ_0 was (0.31 ± 0.04) cm^2/V s. While mobilities as high as 40 cm^2/V s have been reported for rubrene single crystals [7], current in this device is along the slow transport direction of the crystal, thus mobility is not expected to be as high.

The estimated DOS, before and after UVO exposure, are shown in Fig. 6 at three different places along the device: near the bottom contact, in the middle of the crystal, and near the top contact. The figure shows the total concentration of traps—i.e., combining arbitrary, Gaussian, bulk, and local, when appropriate—for the pristine device (#5 C1) and for the UVO treated device (#5 C2). In addition, it also shows the difference between the two DOS in the range 0.2–0.5 eV representing the "extra" concentration of traps required to reproduce the UVO treated device after fixing the rest of the parameters to the result obtained from the pristine device. This extra concentration of traps is only relevant whenever it is comparable or higher than the trap concentration already present in the pristine case, since the model effectively combines all the trap concentrations into a single one regardless of whether they are Gaussian, arbitrary, bulk, or local. It is interesting to note that, even though the model uses a discretized arbitrary trap distribution and it does not make any assumption on its specific shape, the estimated trap distribution induced by UVO can be well approximated by a Gaussian function centered at ~350 meV from the valence band edge with width $\sigma \approx 31$ meV, as shown in Fig. 6.

Note that, while the DOS in the pristine case is essentially described by the piecewise exponential function defined in Fig. 3(a), in the case of the UVO exposed crystal it is composed by the summation of the distribution obtained for the pristine case—fixed in the model—plus the states induced by UVO—which is the function being optimized and is also described by a piecewise exponential. This summation of two exponentials leads to the curved lines in a log scale seen in Fig. 6 when one exponential crosses over the other.

The estimated DOS for the pristine crystal is relatively constant through the semiconductor. The extra concentration of traps near the bottom contact, which accounts for the asymmetry seen in the IV characteristics in Fig. 1, decays very rapidly and is barely noticeable after a few tens of nanometers. The dip in the energetic distribution of traps at 0.2 eV suggests a demarcation in the density of trap states, separating two components: a shallow tail of traps starting at the ME and a deeper concentration of traps around 0.4 eV. Structural disorder has been shown to create a tail of traps that extends from the edge of the band into the band gap [18,19], while chemical defects or impurities are more likely to create traps at discrete energies [20].

Hence, we hypothesize that the DOS for the pristine sample is composed by a shallow tail of traps due to disorder and a deeper concentration of traps created by impurities or chemical defects present in the crystal.

Traps induced by UVO exposure are mostly concentrated near the top surface of the crystal, decreasing towards the

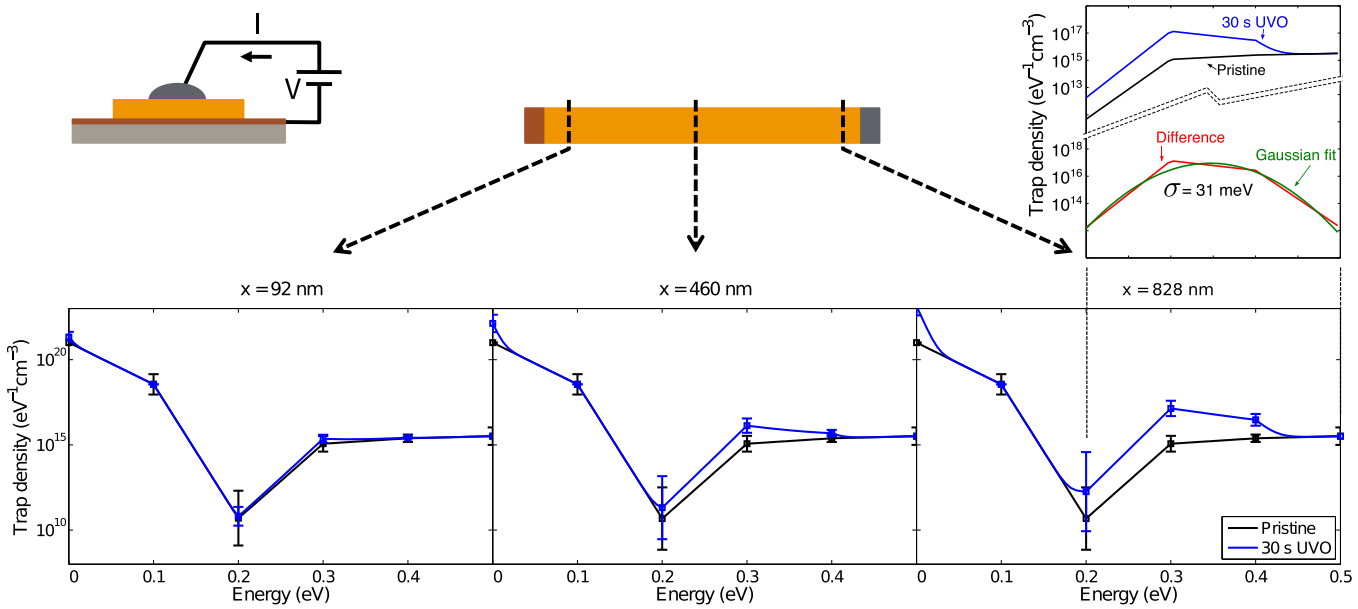

FIG. 6. (Color online) DOS for crystal #5 pristine (C1) and after UVO exposure (C2) at three different locations, from left to right: near the bottom contact, in the middle of the crystal, and near the top contact. The top right plot shows the difference between the estimated DOS for C2 and C1, i.e., the extra DOS induced by UVO exposure, which can be approximated by a Gaussian distribution with $\sigma = 31$ meV.

center of the device and almost inappreciably close to the bottom interface. They are concentrated in a narrow energy range around 0.35 eV, while the tail of traps below 0.2 eV remains essentially unchanged, aside from an apparent peak next to the ME, that is discussed later.

The spatial localization of the induced traps—localized near the top surface—together with the preferred energy level around 0.35 eV, suggest that these states may be related to oxidation of rubrene due to oxygen diffusion through the top surface of the crystal. Figures 7(a) and 7(b) is a sketch of how the UVO treatment affected the rubrene DOS.

Exposure to UVO also increased the concentration of traps near the ME. However, a more thorough analysis reveals that this peak is not real. To start with, no peak near the edge was observed in the absorption spectra measured by photothermal deflection spectroscopy (PDS) measured after exposing a rubrene crystal to UVO (Fig. 8), although the sensitivity of the technique may not have been sufficient.

The cause behind the apparent increase of trap states near the ME can be understood by carefully analyzing what is the effect of the peak on the IV characteristics. Being a narrow peak near the ME, the concentration of carriers in these states and the concentration of mobile carriers (right at the other side of the ME), will have nearly the same temperature and Fermi-level position dependence. Intuitively, the effect of the peak near ME can be described as a reduction of the effective carrier mobility—given by the ratio of mobile to mobile plus trapped carriers next to ME—that mainly affects the current when holes are injected from the exposed surface.

A similar effect occurs if the mobility in the semiconductor is not uniform, but strongly reduced near the top surface. This reduction will mainly affect the forward bias region, i.e., injecting holes from the top contact. Even with a much lower mobility near the top surface, the current at low bias will not be limited, due to the much higher carrier concentration near the contact than in the bulk for low applied voltage.

Hence, by using a position dependent mobility $\mu_0'(x) = w(x)\mu_0$, instead of a constant one, the model is also able to reproduce the original shape. The spatial dependence of the mobility $w(x)$, chosen arbitrarily and optimized to compensate the effect of removing the peak in the trap concentration near the ME, is shown in Fig. 9. However, any shape with a strong spatial dependence will lead to similar results.

Therefore, we hypothesize that the peak of traps near the ME seen in Fig. 6 is an artifact created by the spatially uniform mobility μ_0 through the semiconductor assumed in the model, when in reality the mobility near the top surface will be severely degraded due to UVO exposure.

The decrease of the mobility near the surface of the crystal after UVO is indeed expected. Diffusion of oxygen through the semiconductor and the subsequent formation of $RubO_2$ is likely to disrupt the crystal structure of rubrene, due to the intake of oxygen molecules, thus affecting the free carrier mobility in the material.

IV. X-RAY IRRADIATED CRYSTAL

Damage created by x-ray irradiation on organic semiconductors has been studied in the past mostly on anthracene [21,22], although studies on rubrene have recently appeared [23,24].

Studies of the damage inflicted by irradiation on organic crystals are driven by the possibility to use organic materials as large-scale integrated x-ray imaging panels [23], to understand unintentional damage during x-ray characterization [25], or simply to gain a deeper knowledge of the role of defects on the electrical properties of organic materials by deliberately introducing defects [24]. In this work, it will also serve to

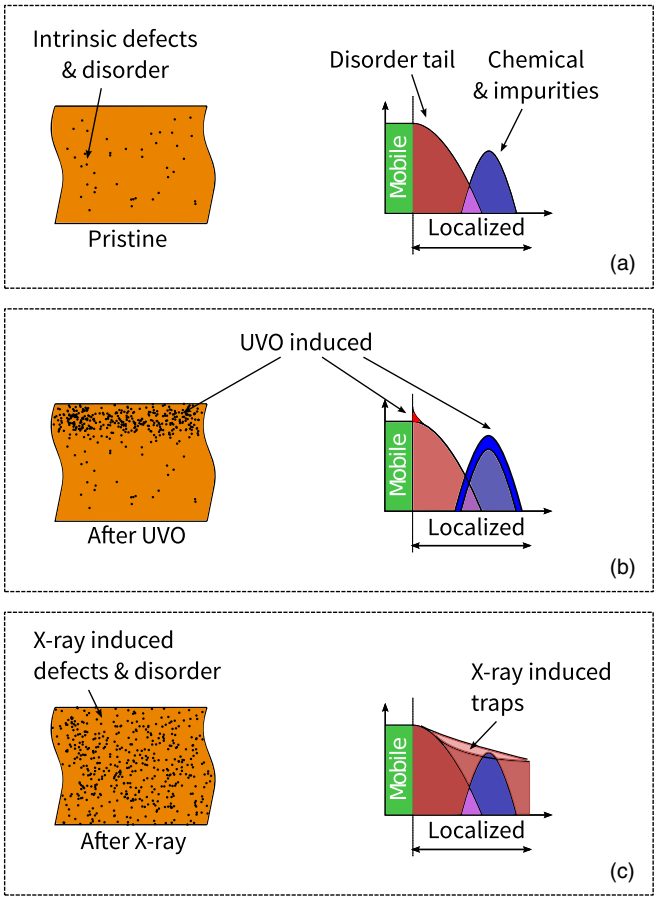

FIG. 7. (Color online) Representation of the effect of UVO exposure on the DOS. (a) DOS for pristine sample is composed of a shallow tail of traps, related to disorder, and a deep region of traps due to chemical and/or impurity related defects. (b) After exposure to UVO, the concentration of traps around 0.35 eV increases; the tail of traps remains unchanged aside from a peak developing right at the ME. (c) After x-ray irradiation, the concentration of traps increases for the entire energy range, consistent with a broadening of the disorder-related tail of traps. Because of this, the dip separating the two trap concentrations around 0.2 eV disappears.

assess whether the proposed numerical model [13,14] is able to distinguish between the electronic properties of defects created by different mechanisms.

The irradiation of a rubrene single crystal has been reported to produce a shift in the onset voltage of TFT with no significant effect in the mobility [24]. The shift in threshold voltage was assigned to the formation of trap states deeper than ∼0.1 eV, although no specific distribution or energy was estimated. As possible causes, it was suggested that ionizing radiation may break the rubrene molecules and produce new chemical species acting as local defects in the crystal structure.

In a different report, TD-SCLC spectroscopy was used to study x-ray damage in rubrene hole-only diodes [23]. It was found that irradiation of rubrene crystals created localized trap states centered at 0.3 eV above the valence band. Annealing the rubrene crystal after x-ray irradiation was shown to partially reduce the previously induced traps, suggesting that at least part of the generated defects are of structural nature. TD-SCLC

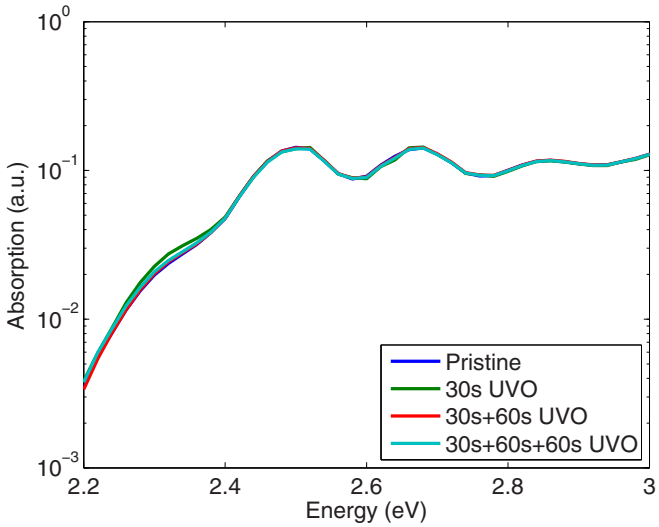

FIG. 8. (Color online) PDS of a rubrene single crystal before and after UVO exposure. No change in the absorption near the band edge is seen even after 150 s (5 times more than the dose used for the electrical measurements). The absorption in the subband-gap region is below the noise level of the setup and is not shown.

spectroscopy does not provide any spatial information, thus the damage was assumed to be uniform thorough the whole crystal. Furthermore, the accuracy of the estimated DOS is likely restricted by the model limitations [13,14]: absence of diffusion current, contact asymmetries, and nonhomogeneity of the trap distribution.

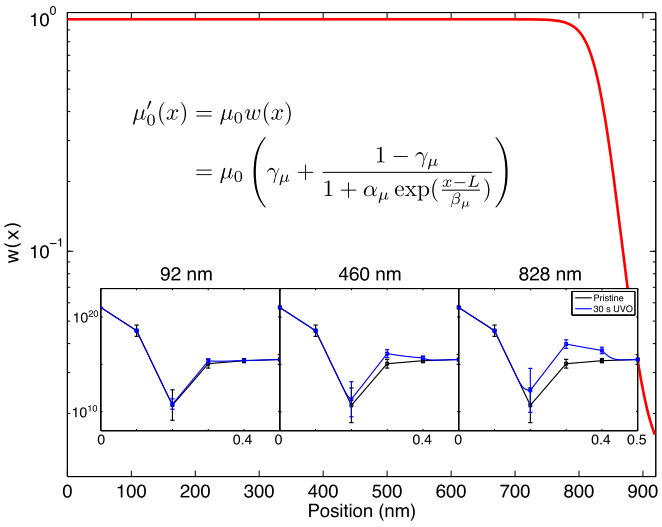

FIG. 9. (Color online) Spatial dependence of the mobility. A strong decrease of the mobility near the top surface, as shown in the figure, has a similar effect on the IV characteristics as a peak in the concentration of traps near the ME. The equation used to describe $\mu_0'(x)$ is shown, however any function with a strong spatial dependence will have a similar effect. Inset shows the trap distribution for the pristine and UVO exposed samples at selected points along the device. Note the absence of any peak near the ME.

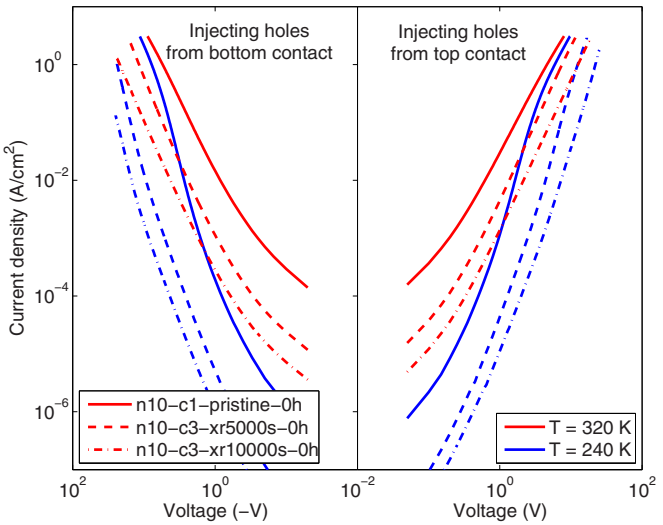

FIG. 10. (Color online) Temperature dependent IV characteristics for crystal #10, devices C1 and C3, before and after x-ray irradiation for 5000 and 10 000 s.

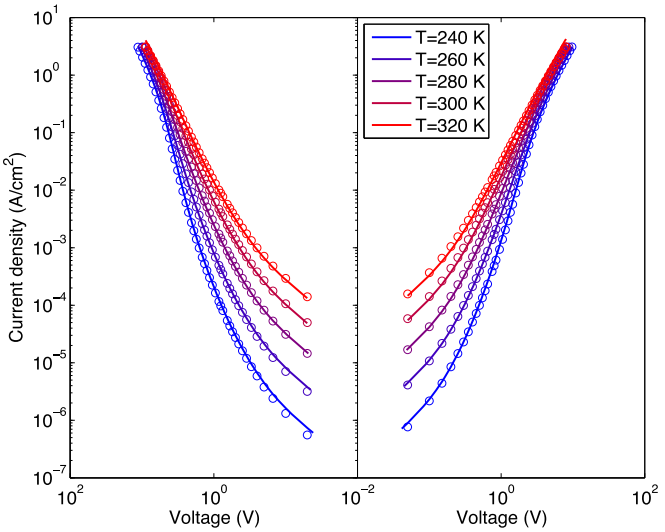

FIG. 11. (Color online) Comparison of measurements (circles) and model fit (solid lines) for crystal #10 C1 (pristine) at different temperatures and bias conditions.

A. Electrical characterization

IV characteristics were taken at different temperatures with the sample in vacuum and in the dark, following a procedure similar to that described before. A drop of water-based graphite was deposited as a contact C1 on top of a pristine rubrene crystal (crystal #10). Similar to the results obtained for crystal #5 (UVO exposed device), injection from the top contact is more efficient than injection from the bottom, leading to an asymmetry in the IV curves.

After measuring the IV curves for the pristine sample, the device was irradiated by exposing it to the x-ray beam of a diffractometer (Cu-$K\alpha$, 45 kV, 40 mA) during 5000 s. A second contact C3 was deposited after irradiation and their IV curves at different temperatures were measured using the same procedure. The device was then irradiated a second time for a total of 10 000 s after which C3 was measured again.

Figure 10 compares the IV measurements before and after x-ray exposure for 5000 and 10 000 s. There are some apparent qualitative differences between the effect of x-ray exposure in Fig. 10 and that of UVO exposure in Fig. 2. While UVO exposure mainly affected the IV curves in the forward bias regime, i.e., injecting holes from the top contact, x-ray exposure affects positive and negative voltages in a similar fashion.

B. Data analysis

The effect of x-ray irradiation on the electrical properties of rubrene was analyzed using the same method described above. First, the model was used to estimate the parameters required to reproduce the IV curves measured for the pristine crystal (#10 C1). Not surprisingly, using the same set of parameters as for device #5 C1—free carrier mobility μ_0, a PWE bulk DOS, and a local Gaussian DOS near the bottom contact—resulted in similar estimated values. The temperature dependent IV curves exhibit excellent agreement between measurements and model, as seen in Fig. 11.

Device C3 (deposited after the first x-ray irradiation), being on the same crystal as C1, is expected to have the same intrinsic properties as measured under C1, except for the changes induced by x-ray irradiation. Therefore, the DOS estimated for device C1 was fixed in C3. The additional free parameters in this case were the carrier mobility and an extra arbitrary (PWE) distribution of traps with a spatial dependence as defined in (1), that accounts for possible traps induced by irradiation. Figures 12 and 13 show the excellent agreement between model and measured IV for #10 C3 after irradiation for 5000 and 10 000 s, respectively.

The estimated DOS for the three cases (pristine and irradiated devices) are compared in Fig. 14 at three different locations along the device: near the bottom, in the middle of the crystal, and near the top contact. Not surprisingly, the DOS for the pristine device #10 C1 is very similar to the DOS estimated for pristine crystal #5 in Fig. 6. In contrast, the estimated energetic and spatial distribution of traps for the

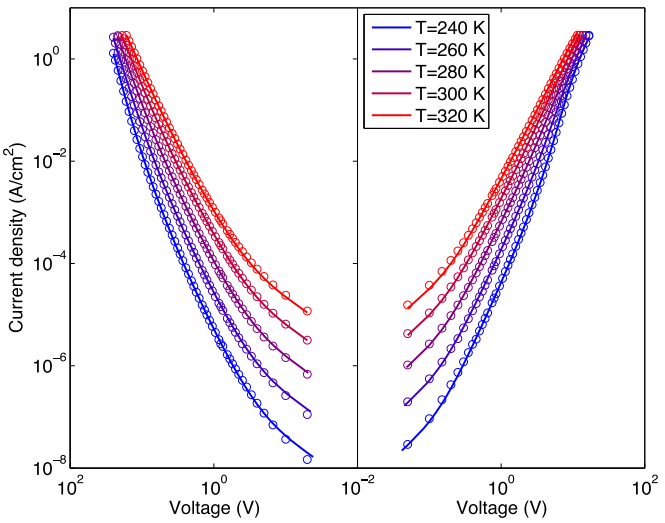

FIG. 12. (Color online) Comparison of measurements (circles) and model fit (solid lines) for crystal #10 C3 after x-ray irradiation for 5000 s.

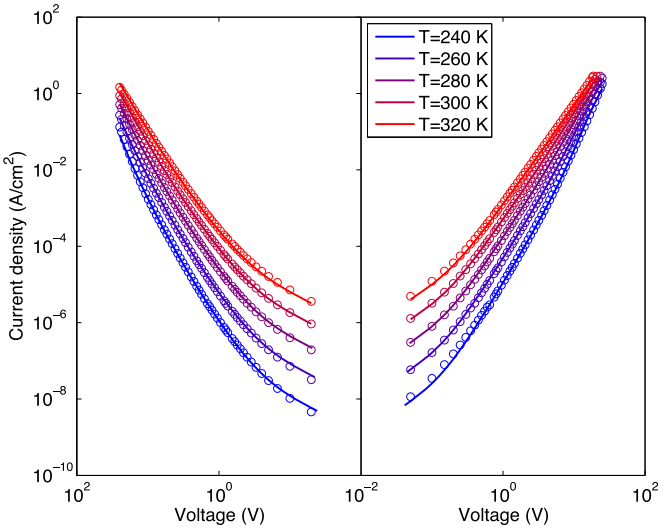

FIG. 13. (Color online) Comparison of measurements (circles) and model fit (solid lines) for crystal #10 C3 after x-ray irradiation for 10 000 s.

irradiated samples—which describe the concentration of traps induced by x-ray irradiation—is significantly different from the trap distribution induced by UVO.

Energy-wise, the density of gap states induced by x-ray irradiation is considerably broader than the states created by UVO—which formed a peak of oxygen-related traps centered at 0.35 eV above the ME. X-ray-induced traps suggest a broadening of the disorder-related tail as depicted in Fig. 7(c). This broadening is consistent with increased concentration of structural defects, such as displacement of molecules, created by absorption of high energy photons. In addition, it agrees with the broad increase of the subgap absorption measured by PDS in x-ray damaged rubrene crystals (see Chap. 14 in Ref. [25]).

Unlike traps created by UVO, the spatial distribution of the x-ray-induced states indicates that a generation of traps extends through the whole semiconductor but is enhanced near the top and bottom interfaces. We note that the traps generated after the first and second x-ray dose have similar energetic and spatial distributions, i.e., broad and featureless energy distribution and spatially enhanced near the interfaces. Device #10 C3 received the first x-ray dose before contact deposition, while the second dose was conducted after contact deposition. Since both doses lead to similar spatial and energetic distribution of traps, we can rule out any significant effect of the contact itself in the generation of traps, which are therefore due to intrinsic semiconductor-radiation interactions.

Possible causes for enhanced trap generation near the surfaces include a preradiation concentration of precursor defects, that evolve into traps after irradiation, or a lower formation energy for structural defects near the surfaces of the crystal.

Note that, although the estimated density of traps around 0.2 eV after the second dose is lower than the result obtained after the first dose, the confidence interval (CI) increased significantly. Hence the result is consistent with a monotonic increase in the trap concentration with the total accumulated

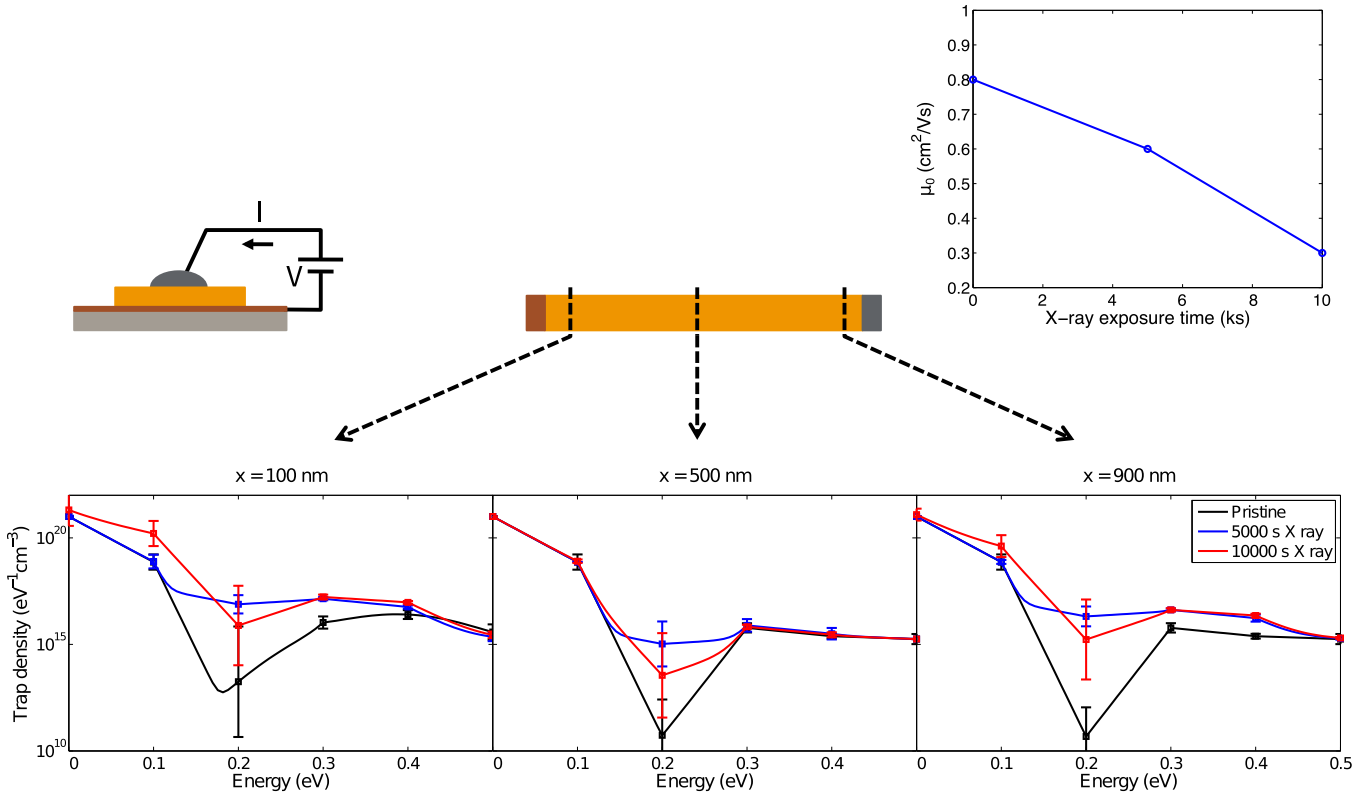

FIG. 14. (Color online) DOS for crystal #10 pristine (C1) and after x-ray irradiation for 5000 and 10 000 s (C3) at three different locations, from left to right: near the bottom contact, in the middle of the crystal, and near the top contact. Top right plot shows the degradation of the mobility with accumulated x-ray dose.

x-ray dose. The reason for the larger CI after the second dose is that, due to the larger concentration of shallow traps around 0.1 eV and because the limited resolution imposed by the Fermi distribution at a finite temperature, the region around 0.2 eV cannot be resolved leading to an increase of the CI. This observation highlights again the importance of calculating proper CI in the estimated parameters if quantitative statements have to be made.

In addition to the creation of traps, x-ray irradiation also led to a monotonic decrease of the mobility as a function of x-ray dose (Fig. 14). The reduction in mobility can be caused by a higher concentration of scattering centers due to increased disorder.

We note that Podzorov *et al.* reported a gradual V_{th} shift in TFT upon x-ray irradiation ascribed to the creation of deep traps (energy deeper than 100 meV above the VB edge). However, contrary to our findings, no changes in mobility were observed [24]. The irradiation was performed by exposing the rubrene crystal to the beam of a Cr x-ray tube with $V = 20$ kV and $I = 10$ mA for up to 330 s. In addition to the likely different effective dose absorbed by the crystal per unit volume, we want to highlight that transport on TFT measured by Podzorov *et al.* and on the unipolar diodes measured in this work occur along orthogonal directions with significantly different transport properties. Furthermore, transport in TFT takes place near the semiconductor-dielectric interface (or the semiconductor surface if an air gap is used as a dielectric) thus being very sensitive to the crystal surface characteristics; while in our diodes carriers flow through the bulk of the semiconductor. For this reason, direct comparison of the effects of x ray on the rubrene transport characteristics are not straightforward.

The mobility obtained for pristine device #10 C1 is about 2.6 times higher than the mobility estimated for pristine crystal #5 C1, which was grown at the same time and identical conditions. In addition to the crystal to crystal variability, there are other sources of errors, not taken into account, that may contribute to the uncertainty in the estimated mobility. For example, the uncertainty in the contact area will affect the estimated mobility if the entire graphite drop does not contact the crystal surface. Even more important will be the crystal thickness—which is estimated as the average of several measurements around the crystal perimeter, and has an estimated error of ∼10%—due to the superlinear relationship between the current in the device and the inverse of the crystal thickness. Given the relatively coarse discretization of the density of states ($\Delta E = 0.1$ eV), variations of ∼10% on the crystal thickness do not significantly affect the resulting trap distribution.

V. CONCLUSIONS

In this work we have used a complete drift-diffusion solver to analyze the effect of UVO exposure and x-ray irradiation on the electrical properties of a rubrene single crystal.

The trap distribution for pristine crystals can be divided into two regions: below and above ∼0.2 eV, where the trap density has a local minimum. The former is ascribed to a structural disorder-related tail of localized states, and decays monotonically as the energy increases. For energies higher than 0.2 eV, the trap concentration increases again and is maximum around 0.3–0.4 eV. Those traps may be caused by chemical defects or impurities (or both) present on the pristine crystal.

Both UVO and x-ray irradiation processes—chosen to intentionally induce defects in the surface and bulk of the rubrene crystal, respectively—were shown to increase the trap concentration in the semiconductor, thus reducing the current in hole-only diodes. However, the utilization of the drift-diffusion model to characterize temperature dependent IV measurements, before and after each process, allows us to estimate the spatial and energetic distribution of the induced traps. In particular, UVO exposure and x-ray irradiation induced traps have very different spatial and energetic signatures.

Upon exposure to UVO, the concentration of trap states in the semiconductor increases near the top surface, while the bottom surface remains unchanged. Its energetic distribution is localized around 0.35 eV. Although the model does not give any information regarding the physical mechanism creating these states, the discrete energy level and the spatial localization near the top surface are consistent with the formation of oxygen-related states due to oxygen diffusion through the top surface.

In addition to the creation of traps, the results suggest that mobility near the top surface is substantially degraded, consistent with a strong disruption of the crystalline structure near the exposed surface, as a result of the oxygen intake.

On the other hand, x-ray irradiation created trap states with a much wider distribution in energy, coherent with a broadening of the disorder-related tail of traps that extends right above the ME. Although x ray are expected to be absorbed uniformly through the crystal, the creation of traps is shown to be more efficient near the top and bottom surfaces. This spatial distribution may suggest that the crystal surface may contain a higher concentration of defects that may be precursors to the radiation-induced trap states; or that the formation energy of vacancies, interstitials, and other structural defects is smaller near the crystal surfaces than in the bulk.

ACKNOWLEDGMENTS

This paper was based on work supported by the Center for Advanced Molecular Photovoltaics (Award No. KUS-C1-015-21), made by King Abdullah University of Science and Technology (KAUST). We would like to thank Professor Daniel Frisbie for providing the materials used in this work.

[1] A. C. Arias, J. D. MacKenzie, I. McCulloch, J. Rivnay, and A. Salleo, Chem. Rev. **110**, 3 (2010).

[2] M. L. Chabinyc, W. S. Wong, A. C. Arias, S. Ready, R. A. Lujan, J. H. Daniel, B. Krusor, R. B. Apte, A. Salleo, and R. A. Street, Proc. IEEE **93**, 1491 (2005).

[3] H. E. Katz and J. Huang, Annu. Rev. Mater. Res. **39**, 71 (2009).

[4] T. W. Kelley, P. F. Baude, C. Gerlach, D. E. Ender, D. Muyres, M. A. Haase, D. E. Vogel, and S. D. Theiss, Chem. Mater. **16**, 4413 (2004).

[5] H. Sirringhaus, Proc. IEEE **97**, 1570 (2009).
[6] R. A. Laudise, C. Kloc, P. G. Simpkins, and T. Siegrist, J. Cryst. Growth **187**, 449 (1998).
[7] T. Hasegawa and J. Takeya, Sci. Technol. Adv. Mater. **10**, 024314 (2009).
[8] O. Mitrofanov, D. V. Lang, C. Kloc, J. M. Wikberg, T. Siegrist, W.-Y. So, M. A. Sergent, and A. P. Ramirez, Phys. Rev. Lett. **97**, 166601 (2006).
[9] C. Krellner, S. Haas, C. Goldmann, K. Pernstich, D. Gundlach, and B. Batlogg, Phys. Rev. B **75**, 245115 (2007).
[10] H. Najafov, D. Mastrogiovanni, E. Garfunkel, L. C. Feldman, and V. Podzorov, Adv. Mater. **23**, 981 (2011).
[11] X. Song, L. Wang, Q. Fan, Y. Wu, H. Wang, C. Liu, N. Liu, J. Zhu, D. Qi, X. Gao, and A. T. S. Wee, Appl. Phys. Lett. **97**, 032106 (2010).
[12] Y. Nakayama, S. Machida, T. Minari, K. Tsukagishi, Y. Noguchi, and H. Ishii, Appl. Phys. Lett. **93**, 173305 (2008).
[13] J. Dacuña and A. Salleo, Phys. Rev. B **84**, 195209 (2011).
[14] J. Dacuña, W. Xie, and A. Salleo, Phys. Rev. B **86**, 115202 (2012).
[15] A. Troisi, J. Chem. Phys. **134**, 034702 (2011).
[16] D. J. Venzon and S. H. T. Moolgavkar, Appl. Stat. **37**, 87 (1988).
[17] P. R. Bevington and D. K. Robinson, *Data Reduction and Error Analysis for the Physical Sciences*, 3rd ed. (McGraw-Hill, Boston, 2003).
[18] R. Noriega, J. Rivnay, K. Vandewal, F. P. V. Koch, N. Stingelin, P. Smith, M. F. Toney, and A. Salleo, Nat. Mater. **12**, 1038 (2013).
[19] J. Rivnay, R. Noriega, J. E. Northrup, R. J. Kline, M. F. Toney, and A. Salleo, Phys. Rev. B **83**, 121306 (2011).
[20] H. Sirringhaus, Adv. Mater. **21**, 3859 (2009).
[21] S. Z. Weisz, J. Chem. Phys. **44**, 1364 (1966).
[22] K. Yokoi and Y. Ohba, Chem. Phys. Lett. **56**, 560 (1978).
[23] T. Morf, S. Haas, T. Zimmerling, and B. Batlogg, arXiv:1303.3831.
[24] V. Podzorov, E. Menard, A. Borissov, V. Kiryukhin, J. A. Rogers, and M. E. Gershenson, Phys. Rev. Lett. **93**, 086602 (2004).
[25] F. Cicoira and C. Santato, *Organic Electronics: Emerging Concepts and Technologies*, edited by F. Cicoira and C. Santato (Wiley-VCH, Berlin, 2013).